Article:
Baghersalimi, G. and O'Farrell, T. (2013) Pilot-aided estimation and equalisation of a Radio-over-Fibre system in Wideband Code Division Multiple Access. IET COMMUNICATIONS, 7 (10). pp. 999-1007. ISSN: 1751-8628

https://doi.org/10.1049/iet-com.2012.0660

Pilot Aided Estimation and Equalisation of a Radio over Fibre System in WCDMA

Gholamreza Baghersalimi* and Timothy O'Farrell**

*Department of Electrical Engineering, University of Guilan, Rasht, Iran, P.O.Box:3756.

Email: bsalimi@guilan.ac.ir

** Department of Electronic & Electrical Engineering, University of Sheffield, Sheffield, Mappin Street, S1 3JD.

Email: t.ofarrell@sheffield.ac.uk

***Abstract*—** In this paper the impact of a Radio over Fibre (RoF) subsystem on the capacity performance of Wideband Code Division Multiple Access (WCDMA) is evaluated. The study investigates the use of pilot aided channel estimation to compensate for the optical subsystem nonlinearities for different channel conditions, estimation intervals, and coding schemes. The results show that pilot aided channel estimation is an effective method for compensating the composite impairments of the optical subsystem and the RF channel. It is found that there is always a suitable pilot power level which maximises the system capacity performance regardless of coding scheme and channel condition. Also, the peak capacity is only slightly affected by a decrease in the estimation interval.

I. INTRODUCTION

Radio-over-Fibre (RoF) is a technology by which information bearing signals using RF (radio frequency) carriers are distributed by means of optical components and techniques. Better coverage and increased capacity, centralised upgrading and adaptation, higher reliability and lower maintenance costs, support for future broadband applications, and economic access to mobile broadband are among the most important advantages of RoF [1,

2, 3]. However, RoF systems are vulnerable to nonlinearities in the optical subsystem that cause degradation of the system performance. The main areas of research in RoF include microwave and millimeter-wave RoF [4, 5, 6], RoF-based Wireless Local Area Networks (WLANs) [7,8], RoF-based cellular systems [8], subcarrier multiplexed RoF systems [8], RoF-based Wavelength Division Multiplexing (WDM) [9] and RoF-based photonic CDMA [10]. In particular, estimation methods, modelling the radio subsystem, modelling the optical subsystem and multiple access techniques are regarded as the most important investigation topics in this context.

Channel estimation is a subject which has received a great deal of attention by researchers in recent years. In wireless systems, channel estimation techniques are used for the estimation of the RF channel impulse response (CIR) in order to compensate for the amplitude distortion and phase rotation introduced by the RF channel variations. In cellular communication, estimation is achieved by time-multiplexed pilot signals, code-multiplexed pilot signals, or a combination of these signals. In the wireless LAN systems, on the other hand, estimation is carried out by frequency (subcarrier) multiplexed pilot signals, time (symbol) multiplexed pilot signals, or a combination of these signals [11]. All such equalisation techniques require extra hardware at either the transmit and/or the receive side of the communication link.

For RoF-based wireless communications, there is a dearth of publications in the context of channel estimation and compensation [2- 8, 12, 13, 14]. In particular, for more realistic conditions the collective effects of modulation, channel coding, multiuser interference (MUI), large signal distortion, RF channel distortion, data rate, diversity, estimation level and equalisation techniques have not been substantially investigated before.

It should be emphasised that both the amplitude and phase distortions of an optical channel affect the system performance. Also, due to the hysteresis-type memory of the optical subsystem, the entire RoF link suffers more from the phase impairments and frequency-dependent nonlinearities when compared to a nonlinear element such as an RF High Power Amplifier (HPA) as used in cellular mobile or satellite communications.

In this paper, the impact of the optical subsystem nonlinearities on the performance of a downlink Wideband Code Division Multiple Access (WCDMA) cellular mobile system is studied in respect of the channel estimation and equalisation functions. Results for the WCDMA system capacity performance are presented for different channel conditions, coding schemes and estimation intervals when a code multiplexed Common PIlot CHannel

(CPICH) is used to compensate for the distortion introduced by both the optical channel and the RF channel, i.e. a combined nonlinear time-variant channel. Strictly speaking, the overall nonlinear time-variant subsystem (optical subsystem plus RF channel) is linearly estimated and equalised using CPICH under different conditions. Also, as this research focuses only on the optical subsystem, other sources of nonlinearity, such as the RF HPA, are not considered.

The paper is organised as follows. Section II introduces the theoretical background for estimating and equalising the optical subsystem. Section III presents the computer simulation model while Section IV presents the salient results and discussion of results. Finally, Section V concludes the paper.

II. SYSTEM MODEL AND ANALYSIS

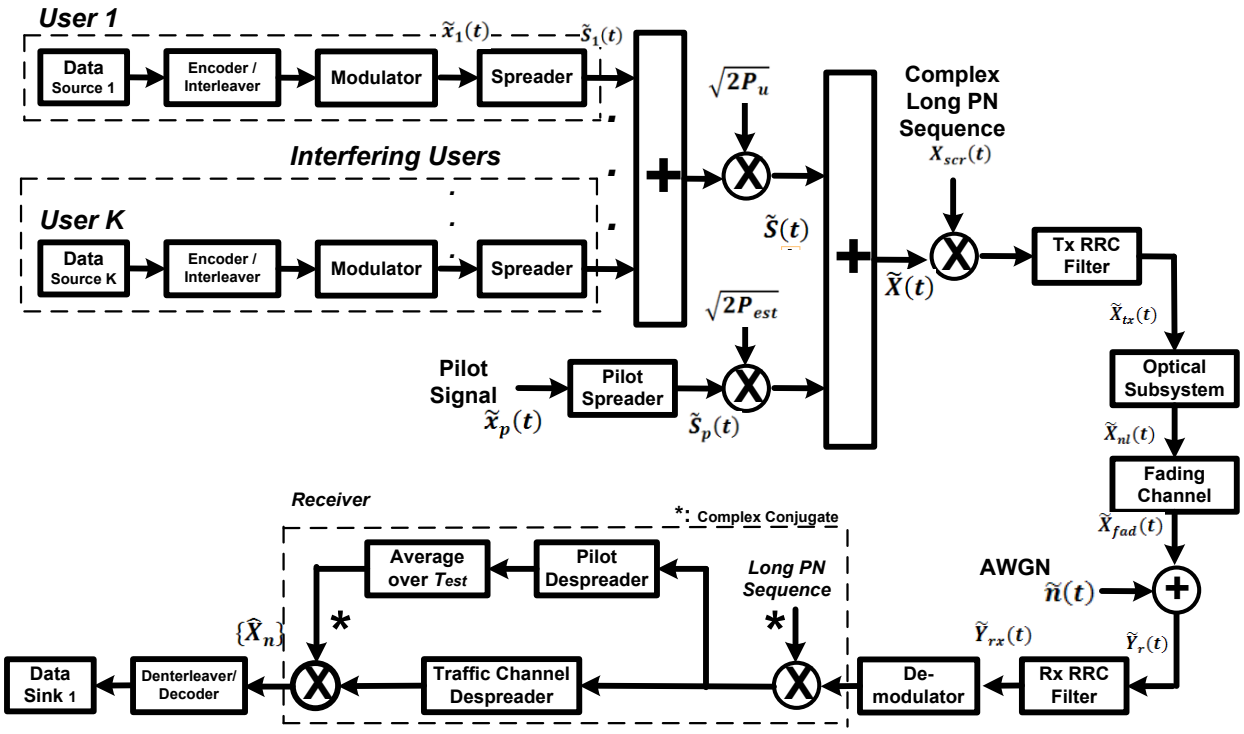

Fig. 1 Downlink RoF-WCDMA System Model.

In this section, the mathematical background of the baseband RoF WCDMA model, which is shown in Fig. 1, is described. In general, this model comprises a transmitter, an optical link, an RF channel and a receiver. These subsystems are described in the following subsections.

A. Transmitter

Each user in the RoF-WCDMA system independently sends its data bit stream to the channel encoder. This block may be a rate 1/3 Convolutional Encoder (CC) or a rate 1/3 Turbo Encoder (TC). Then, an interleaver is applied for an effective use of the channel encoders. Thereafter, the interleaved data enters the modulator where they are converted to a symbol train using the QPSK mapping rule. Let the k th user signal over the frame period T_{fr} be denoted by[1]

$$\tilde{x}_k(t) = \sum_{n=1}^{N_s} X_{k,n}\, \delta(t-(n-1)T_s); \qquad 0 \le t \le T_{fr} \tag{1}$$

where $X_{k,n} = b_{k,n} + jd_{k,n}$ is the n th symbol of the k th user, $b_{k,n}$ is the n th symbol's in phase component of the k-th user, $d_{k,n}$ is the n th symbol's quadrature component of the k th user, T_s is the symbol period for all users, N_s is the number of data symbols being transmitted for each user in the frame period $T_{fr} = N_s T_s$, and $\delta(t)$ is the Dirac delta function. In the above relationship, it is assumed that all users transmit at the same data rate, or equivalently, have the same spreading factor. Without loss of generality, in order to simplify the notation it is assumed that the first user is the intended user, so that the intended user's signal over the frame period ($0 \le t \le T_{fr}$), with unit power, can be written without the index $k = 1$ as shown in Eq. 2.

$$\tilde{x}_1(t) = \sum_{n=1}^{N_s} X_n\, \delta(t-(n-1)T_s) = \sum_{n=1}^{N_s} (b_n + jd_n)\, \delta(t-(n-1)T_s) \tag{2}$$

Each information bearing signal is then multiplied by the corresponding spreading sequence, as described by Eq. 3

$$g_k(t) = \sum_{m=1}^{SF} c_{k,m}\, \delta(t-(m-1)T_{ch}); \qquad 0 \le t \le T_s \tag{3}$$

[1] Hereafter, all baseband signals are denoted using a tilde ~.

where *SF* is the data spreading factor which is assumed to be the same for all users, T_{ch} is the chip duration and $c_{k,m}$: *m*=1, 2,…, *SF* is the *m*-th element (chip) of the *k*-th user's binary spreading sequence. The spreading sequences are chosen from the Walsh Hadamard (WH) sequences which are mutually orthogonal [15]. In addition, if the spread signal of the *k* th user over a whole frame interval is denoted by Eq. 4,

$$\begin{aligned} \widetilde{z}_k(t) &= \sum_{n=1}^{N_s}\sum_{m=1}^{SF} c_{k,m}\,\delta(t-(n-1)T_s-(m-1)T_{ch}) \\ &= \sum_{n=1}^{N_s} g_k(t-(n-1)T_s); \qquad 0 \le t \le T_{fr} \end{aligned} \tag{4}$$

then the *k* th user spread signal of average power P_k and the total multiuser spread signal over the same frame interval can be represented, respectively, by Eq. 5 and Eq. 6

$$\widetilde{S}_k(t) = \sum_{n=1}^{N_s} X_{k,n}\, g_k(t-(n-1)T_s) \tag{5}$$

$$\widetilde{S}_K(t) = \sum_{k=1}^{K}\sum_{n=1}^{N_s} \sqrt{2P_k}\,[X_{k,n} g_k(t-(n-1)T_s)] \tag{6}$$

where *K* is the total number of users. Then, the CPICH is added to the transmitted signal in order to provide a channel estimation mechanism. The spreading sequence of this signal is defined by Eq. 7

$$g_p(t) = \sum_{i=1}^{SF_p} q_i\,\delta(t-(i-1)T_{ch}); \qquad 0 \le t \le T_p \tag{7}$$

where SF_p is the spreading factor of the pilot signal, q_i: *i*=1, 2, …, SF_p is the *i*-th element of the spreading sequence of the pilot signal and T_p is the duration of a pilot symbol. Also, the transmit pilot symbol sequence (i.e. the non-spread pilot signal) can be represented by Eq. 8

$$\widetilde{x}_p(t) = \sum_{j=1}^{N_p} a_j\,\delta(t-(j-1)T_p); \qquad 0 \le t \le T_{fr} \tag{8}$$

where a_j is the *j*-th transmit pilot symbol and N_p is the number of pilot symbols per frame, hence $T_{fr} = N_p T_p$. Therefore, the spread pilot signal over a frame time, which is known to the receiver, can be described by Eq. 9.

$$\widetilde{S}_p(t) = \sum_{j=1}^{N_p} a_j \, g_p(t-(j-1)T_p); \qquad 0 \le t \le T_{fr} \tag{9}$$

Hence, the total transmit signal over a frame is given by

$$\widetilde{X}(t) = \sum_{k=1}^{K} \sum_{n=1}^{N_s} \sqrt{2P_k}\,[X_{k,n} g_k(t-(n-1)T_s)] + \sqrt{2P_{est}}\,\widetilde{S}_p(t) \tag{10}$$

where P_{est} is the average power of the pilot signal. In this paper, all users are assumed to transmit with equal power P_u (i.e. $P_k = P_u$; $k=1,2,\ldots,K$) which is the average power of a user for a certain service. By defining parameter R as the ratio of the pilot power P_{est} to the total transmit power P_{t} as shown in Eq. 11,

$$R = \frac{P_{est}}{P_t} \tag{11}$$

then the total transmit power is given by Eq. 12

$$P_t = KP_u + P_{est} \tag{12}$$

where the number of users K is given by Eq. 13.

$$K = \lfloor SF \times \eta_0 \times (1-R) \rfloor \tag{13}$$

The term in $\lfloor x \rfloor$ denotes the largest integer not greater than x and η_0 denotes the cell load factor. The parameter R must be chosen in order to achieve reliable detection at the receiver without consuming excess resources and hence capacity within the cellular system. Subsequently, the total spread signal is multiplied by the complex long PN sequence or scrambling code. The long-PN sequence is applied on top of the channelisation codes and, on the downlink, is used jointly to separate different cells of the cellular WCDMA system and to mitigate multipath. The long-PN sequence does not alter the chip rate of the spread signal [15]. Following multiplication by the complex long-PN sequence, the resultant signal is up-sampled and filtered by the transmit RRC (root raised cosine) filter as shown in Eq. 14

$$\widetilde{X}_{tx}(t) = h_{rrc}(t) * [\widetilde{X}(t) \times X_{scr}(t)] \tag{14}$$

where * denotes convolution and $h_{rrc}(t)$ denotes the impulse response of the RRC filter, with roll-off factor equal to 0.22 and oversampling factor equal to 4. Term $X_{scr}(t)$ is the complex long-PN sequence or scrambling code.

B. Optical Subsystem

In the analysis of communication systems, analytic models of subsystems are preferred because they normally lead to closed form analytic solutions for the system. However, these models are only valid under certain conditions and assumptions. In addition, some analytic techniques such as the Volterra series approach (for nonlinear systems with memory such as the laser diode which is described by the rate equations) are very difficult to treat. Further, in some cases the physical problems cannot be represented by mathematical models. One alternative for describing such complex systems is behavioural modelling. In behavioural modelling, the system is treated as a black box with transfer characteristics described by a set of equations. For an optical system, the transfer characteristics are expressed as AM AM (amplitude-to-amplitude) and AM PM (amplitude-to-phase) characteristics (also known as the large-signal response). The former is an amplitude transfer function while the latter is a phase transfer function. The black box model accounts for the composite effects of all impairments in the system such as static and dynamic nonlinearities and optical noise. The main advantage of behavioural modelling is that it can describe a complex system without needing to have a detailed knowledge of its constituent subsystems or components.

The use of AM-AM/PM models is based on the underlying assumption that the envelope of the signal is varying slowly such that the model, rather than the instantaneous value of signal, is used.

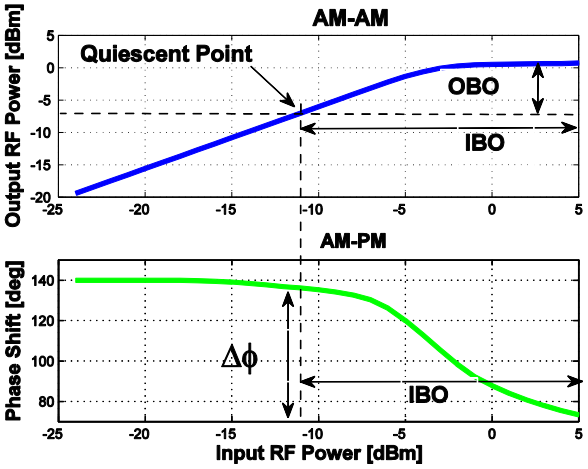

Fig. 2 AM AM/PM Characteristics (IBO: Input Back-off).

The models are valid when the device "memory time" (amplitude- and frequency-dependent time delay between the transmitted and received RF signal) is much smaller than the reciprocal of the input signal bandwidth [16]. In other words, these characteristics can be used only when the nonlinear system is treated as a quasi-memoryless system [17]. As a rule of thumb, the AM-AM/PM models are used when the memory of the nonlinear system is at least twice less than the reciprocal of the envelope frequency [16, 18]. This condition is met in this study.

The optical subsystem used in this research comprises an LD (laser diode), a 2.2 km long single-mode fibre and a PD (photodiode). The optical transmitter used is a directly modulated InGaAsP DFB (distributed feedback) LD with an operating wavelength of 1310 nm. Also, the optical receiver consists of an overall 32 dB gain which completely compensates for the total loss of this optical link. The radio frequency is 1.8 GHz, though the frequency response of the link is flat over frequencies $1.7 < f < 2.2$ GHz. The AM-AM/PM transfer functions are shown in Fig. 2. Further, a pictorial description of OBO (output back-off) is shown in Fig. 2 and is defined (on a logarithmic scale) as the difference between the maximum output power and the output power at the quiescent operating point.

The RRC filtered signal passes through the nonlinear (*nl*) optical subsystem whose output is given by Eq. 15

$$\widetilde{X}_{nl}(t) = G_{out}\sqrt{\frac{2}{R_{out}} f_{AM-AM}(0.5R_{in}(G_{in}\left|\widetilde{X}_{tx}(t)\right|)^2)} \times \exp[jf_{AM-PM}(0.5R_{in}(G_{in}\left|\widetilde{X}_{tx}(t)\right|)^2 + j\psi_{\widetilde{X}_{tx}}(t)] \tag{15}$$

where $G_{in} = \sqrt{\frac{\max(P_{RF,i})}{IBO \times P_m}}$ is the gain of the pre-amplifier which matches the output power of the transmit RRC filter to the input power of the optical subsystem [8], IBO is the input back-off on a linear scale, P_m is the maximum input RF power to the optical subsystem before the pre-amplifier, $\max(P_{RF,i})$ is the (measured) maximum input RF power before the pre-amplifier, $\psi_{\tilde{X}_{tx}}(t)$ is the phase of the signal $\tilde{X}_{tx}(t)$, $R_{in} = 50\,\Omega$ is the input impedance of the optical subsystem, $R_{out} = 50\,\Omega$ is the output impedance of the optical subsystem, and G_{out} is a linear gain which sets the overall gain of the optical subsystem to unity. Also, $f_{AM-AM}(.)$ and $f_{AM-PM}(.)$ are the AM AM and AM PM transfer function characteristics of the nonlinear (optical) subsystem, respectively.

C. RF Channel

Following the optical subsystem, the signal passes through the RF fading channel. A new set of fading taps are generated every T_{fr} seconds using a unit variance complex Gaussian process. The output signal of the fading block can be represented as Eq. 16

$$\tilde{X}_{fad}(t) = \sum_{l=1}^{L} \tilde{a}_l(t)\tilde{X}_{nl}(t-\tau_l) = \sum_{l=1}^{L} R_l(t)e^{j\varphi_l(t)}\tilde{X}_{nl}(t-\tau_l) \tag{16}$$

where L is the number of multipaths, $\tilde{a}_l$ is the complex gain of the l th path, τ_l is the excess delay of the l th path, while $R_l = |\tilde{a}_l|$ and φ_l are the magnitude and phase, respectively, of the complex gain $\tilde{a}_l$. In general, the path amplitudes, phases and delays are time dependent. Also, the terms in $\tilde{a}_l$ are normalised such that the average received power is unity, i.e. $E[P_l] = \sum_{i=1}^{L} E\left[|\tilde{a}_l|^2\right] = 1$ and E[·] denotes the expectation operator. Hence, the received average power level is not affected by the fading channel. E_b is defined as the average bit energy of the intended user while the signals from other users are treated as an MUI. Thus, Eq. 16 can be rewritten as Eq. 17

$$\tilde{X}_{nl}(t) = \tilde{x}_{s1}(t) + \tilde{n}_d(t) \tag{17}$$

where $\widetilde{x}_{s1}(t)$ is the scrambled and up-sampled (and possibly amplified/attenuated) version of signal $\widetilde{S}_1(t)$, and $\widetilde{n}_d(t)$ is the total distortion introduced by the multipath fading , optical subsystem , and other users.

After the fading channel is applied, the signal is perturbed by a zero-mean complex AWGN process $\widetilde{n}(t)$. So, the received signal can be represented by Eq. 18.

$$\widetilde{Y}_r(t) = \widetilde{x}_{s1}(t) + \widetilde{n}_d(t) + \widetilde{n}(t) \tag{18}$$

Then, the signal-to-interference-noise ratio (SINR) is given by Eq. 19.

$$SINR = \frac{E[\widetilde{x}_{s1}{}^2(t)]}{E[\widetilde{n}_d{}^2(t) + \widetilde{n}^2(t)]} \tag{19}$$

D. Receiver

At the receiver, the noise perturbed signal is filtered by the receive RRC filter followed by down-sampling, where the output of this filter is given by Eq. 20.

$$\widetilde{Y}_{rx}(t) = h_{rrc}(t) * \widetilde{Y}_r(t) \tag{20}$$

In this paper, the joint optical and RF channels are estimated using a pilot symbol channel estimation technique. That is, pilot symbols are used to train sequences for estimating the combined optical and RF channel impulse response. To do so, a perfect knowledge of the delays of different paths is assumed.

In general, by using post correlation compensation all the paths or taps are estimated and averaged over the estimation time T_{est} (which is shorter than T_{fr}) according to a strategy to give a complex tap estimate for that particular interval. Then all complex taps are applied to the data signal in the corresponding time intervals in the same path. This process is repeated for all time intervals per frame and for all paths. For example, in [15] a multi slot (each slot corresponds to 1/15 th of a frame duration) Moving Window Averaging (MWA) filter was used to determine the final channel estimate in a particular slot. Thereafter, each final estimate per slot was used to compensate for the channel impairment in the corresponding data slot. As another example, a 6 symbol MWA filter was used in [19] to obtain the final channel estimate per symbol. Then, each final estimate per symbol was applied to the corresponding data symbol.

In this paper, a channel estimate is obtained during the interval T_{est} , and then applied to the whole frame. In other words, after deriving the channel estimate it is immediately applied to the entire data frame. This approach reduces the processing time and complexity of the receiver. The tap extraction process comprises three vector multiplications (i.e. the scrambling code, pilot spreading code and transmit pilot) followed by an integration over T_{est}. The shorter the estimation time the shorter the length of the three vectors, hence a more time efficient process can be achieved. Nonetheless, averaging over longer periods gives better estimates of the channel. This concept is investigated using capacity as the main metric for different estimation durations including frame, slot, and symbol periods. The estimated tap in path *l* can be represented by Eq. 21.

$$\hat{\tilde{a}}_l = \int_0^{T_{est}} \tilde{Y}_{rx}(t-\tau_l) X_{scr}(t-\tau_l)^* \tilde{S}_p(t-\tau_l)^* dt \tag{21}$$

After applying the estimated tap for each path to the data signal in each frame, the resultant compensated data are combined. In this study, the Maximum Ratio Combiner (MRC) is used. The signal in each path is multiplied by the conjugate of the estimated tap which is proportional to the signal power in the same path. This was shown to give the best performance compared to other combining rules [15]. Therefore, the *n* th received symbol for intended user-1 in the time interval $nT_s \le t \le (n-1)T_s$, as denoted by $\hat{X}_n$, may be represented by Eq. 23.

$$\hat{X}_n = \sum_{l=1}^{L} \hat{\tilde{a}}_l^* \int_{(n-1)T_s}^{nT_s} \tilde{Y}_{rx}(t-\tau_l) X_{scr}(t-\tau_l)^* \tilde{Z}_1(t-\tau_l) dt = \hat{b}_n + j\hat{d}_n \tag{22}$$

The term $\tilde{Z}_1(t)$ denotes the spreading waveform of user-1 while the terms in $\hat{b}_n$ and $\hat{d}_n$ are the in phase and quadrature components, respectively, of user-1's *n* th estimated symbol. The soft outputs of the demodulator are then passed to the deinterleaver in order to rearrange the demodulated data. The data stream is then decoded according to the channel coding used at the transmit side. Following decoding, the data bits are collected at the data sink and compared to those transmitted.

It should be emphasised that the value of the proposed estimation method compared with previous studies in the literature –addressed in Section I, paragraph 3- is that by using existing channel estimation and correction techniques, the distortion due to the optical subsystem can be accommodated without using extra hardware at either

the transmit and/or the receive side of the communication link. Also the comprehensive nature of the study which models the collective effects of the modulation, coding, multiple user interference, large signal distortion, multipath propagation as well as channel estimation and equalisation contribute to the unique value of the work undertaken.

III. SIMULATION SETUP

In order to evaluate the effects of the optical subsystem on WCDMA, computer simulations were carried out based on the system model presented in Fig. 1. In this arrangement the total power, which is the sum of the powers of all spread signals including the pilot signal, is divided between the pilot signal and the users. This can be represented mathematically by Eq. 23 where $0 < \left(R = P_{est} / P_t\right) < 1$

$$\frac{P_{est}}{P_{users}} = \frac{RP_t}{(1-R)P_t} = \frac{R}{1-R} \tag{23}$$

where $P_{users} = KP_u$ is the total transmit power of all the users.

A key performance metric for WCDMA is the continuous-user (channel) capacity, which is defined as the maximum number of users (or channels) that can be provided in a fixed frequency band [20]. This capacity is also a metric of the spectrum efficiency of a wireless system for either the uplink or downlink. In a cellular CDMA system, capacity is calculated at an operating E_b / N_o [20] as given by Eq. 24

$$C = \eta_0 \times \frac{1 + G_p (E_b / N_0)^{-1}}{\alpha(1+\rho)} \tag{24}$$

where G_p is the processing gain (i.e. the ratio of the chip rate to the data rate), η_0 is the cell load factor , α is the activity factor of the data signal, and ρ is the intercell to intracell interference ratio. As the end user of an RoF network utilises the spectrum of the wireless channel, the same capacity concept can be applied for such networks. In this research, each user corresponds to a 40 kbit/s data rate.

In this paper, a single cell system is considered with all the mobiles active all the time, hence $\alpha = 1$ and $\rho = 0$. The cell load factor η_0 is defined as the ratio of the number of users to the maximum allowable number of users,

which is determined by the spreading factor *SF*. In addition, a proportion of the transmit power is dedicated to the pilot signal. Since the factor *R* is the ratio of the pilot power to the total transmit power and as all the users have the same transmit power, then the cell load factor is given by $\eta_0 = 1 - R$. Therefore, the capacity of the cellular system is given by Eq. 25.

$$C = (1-R)\left[1 + \frac{G_p}{E_b/N_0}\right] \tag{25}$$

Finally, RF channel parameters [21], WCDMA system parameters [22], [23], and optical subsystem parameters [12] are summarised in Tables I, II, and III, respectively.

TABLE I

RF CHANNEL PARAMETERS

Case	Delay Profile [ns]	Power Profile [dB]	Speed (km/h)
Flat	[0]	[0]	50
3-Path	[0 976 20000]	[0 0 0]	3
4-Path	[0 260 521 781]	[0 -3 -6 -9]	120

TABLE II

WCDMA SYSTEM PARAMETERS

Quantity	Value
Frame Length	10 ms (=400 bits)
Data Rate	40 kbps
Channel Interleaver Depth	10 ms
Number of Frames	600
Chip Rate	3.84 Mcps
Spreading Factor	Data: 64, Pilot: 256
Estimation Level	Frame: 10 ms
	Slot: 0.667 ms
	Symbol: 0.0167 ms
Coding	I-Convolutional
(Rate =1/3)	II-Turbo
	Constraint Length: K_{CL} = 4
	Decoding: Max Log MAP
	Number of Iterations: 6

TC Internal Interleaver Depth	Baseline 10 ms all channels plus 80 ms for 3-path channel
Ratio of Pilot Power to Total Power R [%]	0.003, 0.005, 0.01, 0.03, 0.1, 1, 1.5 , 3, 10, 20, 40, 60 , 80
Target BER	10^{-3}
Confidence Interval	95%

TABLE III
OPTICAL SUBSYSTEM PARAMETERS

Quantity	Value
Output Back off	0, 0.3, 3 dB
Max($P_{RF,i}$) [ref. value for OBO]	3.1623 mW (≡ 5 dBm)
Wavelength	1310 +/- 10 nm
Modulation Gain	0.12 mW/mA
PD Responsivity	0.75 mA/mW
Fibre Type	Single-Mode (9/125)
Fibre Length	2.2 km
Post-Amplifier Gain	32 dB
Overall Gain	0 dB
LD Type	DFB

IV. RESULTS AND DISCUSSION

The continuous user capacity performance (Eq. 25) is evaluated for different cases including CC/FF (convolutional code / flat fading), TC/FF (turbo code/flat fading), TC/FS(3 path) (turbo code/3-path frequency selective fading), with different interleaver depths, and TC/FS(4 path) (turbo code/4-path frequency selective fading) all dimensioned at the frame level. Also, for the TC/FS(4 path) case both slot and symbol level channel estimations are compared.

A. The Effect on Capacity of the Coding Scheme

Fig. 3 plots capacity versus P_{rel} in dB for the CC/FF scenario, where $P_{rel} = P_{est} / P_u$ is the relative power of the pilot signal to that of a single user (P_u). Results are shown for OBO levels 0, 0.3, and 3 dB and a target BER of 10^{-3}. The capacity graphs have three distinct regions: Region I - the capacity increases with increasing R from zero to a

specified value R_1 (i.e. $0 < R \le R_1$); Region II – the capacity plateaus as R is increases from R_1 to R_2 (i.e. $R_1 < R \le R_2$); and Region III – the capacity decreases as R increases (i.e. $R_2 < R$).

This behavior may be explained more accurately as follows. In the nonlinear RoF WCDMA system, unlike the linear system, the orthogonality of the wanted user's spreading code (i.e. user-1) to that of the pilot signal and also to each spreading code of the other users is lost. When R is small, the pilot power (P_{est}) is low while the MUI is high which gives a very noisy estimate of the channel impairment. For this case, the system BER, and hence capacity, degrades rapidly. When R is large, the pilot power is high while the MUI is low. Though this case provides a good channel estimate, the excessive interference power contributed by the pilot signal degrades the channel capacity. For this case the system BER degrades, but less rapidly than the case when R is small. The interaction of the pilot power and MUI clearly leads to an optimum value for R which minimises the BER and maximises the capacity.

As explained, the BER performance is improved by increasing R to a specific value. This behavior implies that the required E_b/N_0 to achieve the target BER of 10^{-3} decreases as R increases (corresponding to Regions I of Fig. 3). For this case, the factors (1 R) and E_b/N_0 in Eq. 25 for determining capacity decrease; the former decreases linearly while the latter decreases nonlinearly. In region II, the required E_b/N_0 changes slightly. For this case, there is a balance between the factors (1 R) and E_b/N_0. With a further increase in R, the BER performance degrades, consequently the required E_b/N_0 for the same target BER increases. For this case (i.e. region III), the factor (1-R) decreases linearly while E_b/N_0 increases nonlinearly. The interaction of the two trends results in an optimum value of R which maximises the capacity C. For the CC/FF case, the optimum value of R is in the range $0.3\% < R < 3\%$. The above argument holds for all OBO levels regardless of the coding scheme. To verify this point, further simulations were carried out using a TC as the channel code. The corresponding capacity graphs are shown in Fig. 4 where the same capacity trend is obtained as in the CC case. However, the TC achieves a slightly higher capacity performance than the CC. This slight improvement, which is primarily due to the depth of the TC internal interleaver, is justified in Subsection C.

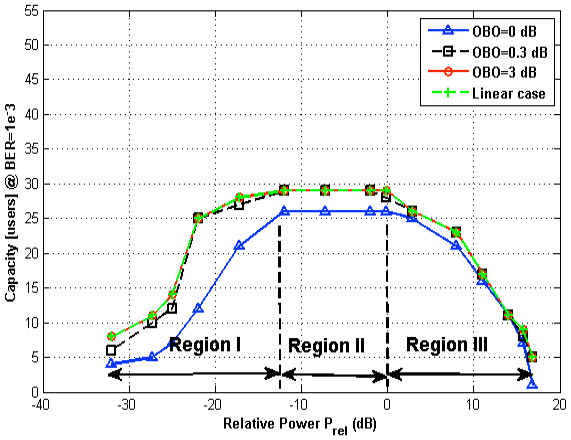

Fig. 3 Capacity vs. P_{rel} for a CC/FF Scenario

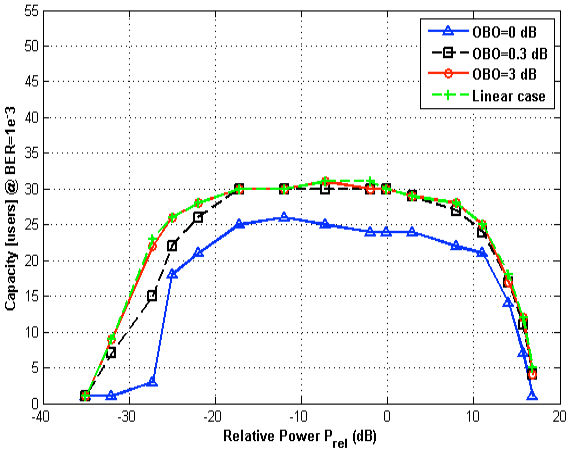

Fig. 4 Capacity vs. P_{rel} for a TC/FF Scenario: 10 ms Interleaver Depth

B. Frequency Selective Fading

To study the effect of fading channel type on the capacity performance, simulations were carried out for the TC/FS(3-path) case. The results are shown in Fig. 5 for a 10 ms interleaver depth. The results indicate that the same mechanisms described in Subsection A also determine the capacity performance in the TC/FS(3-path) scenario. Consequently, there is always an optimum R which maximises the system capacity performance. However, the capacity for this case is improved in comparison to the flat fading case due to frequency diversity. This fact will be

evidenced further in Subsection D. Also, compared with the flat fading performance the results in Fig. 5 for frequency selective fading demonstrate a proportionally greater capacity degradation at 0 dB OBO.

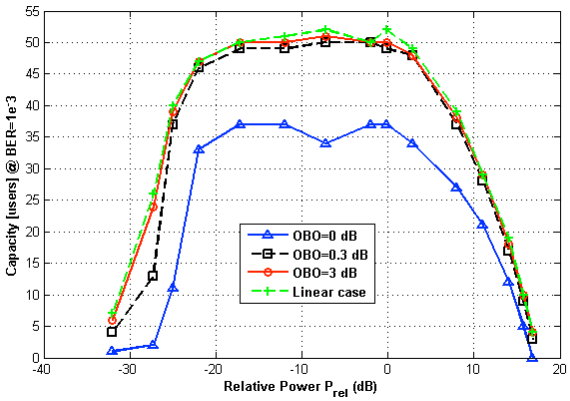

Fig. 5 Capacity vs. P_{rel} for TC/FS(3 Path) Case: 10 ms Interleaver Depth

C. The Effect of TC Internal Interleaver Depth

In Turbo coding interleaving is used to randomise the bit stream to achieve an effective use of the channel encoders, which in turn leads to a capacity performance improvement. In Subsection B, the interleaver depth and TC block size was investigated for 10 ms. In order to evaluate the effect of the TC block and interleaver depth on the system performance, the previous experiments were repeated with an interleaver depth of 80 msec for the 3-path FS channel. The resultant capacity plots are shown in Fig. 6, in which the channel estimation is performed at the frame level. The general trends for all graphs are similar to the primary results in Fig. 5 for a 10 ms interleaver depth. The effectiveness of the interleaver is substantially enhanced by increasing its depth. At 0 dB OBO (the worst case nonlinear scenario), for example, the peak capacity with 10 ms interleaver depth is 37 users and remains above 30 users for $-23 < P_{rel} < 5$ dB, while with 80 ms interleaver depth the peak capacity increases to 39 users and remains above 30 users for $-30 < P_{rel} < 9$ dB). This corresponds to a peak capacity improvement of 5.4%, but more importantly the operating range of P_{est} is significantly increased.

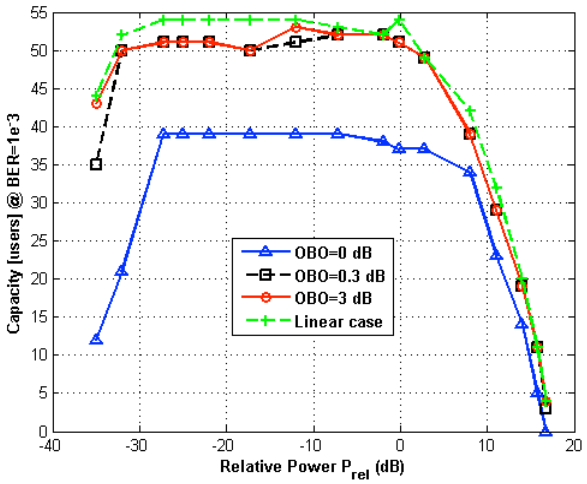

Fig. 6 Capacity vs. P_{rel} for TC/FS(3 Path) Case: 80 ms Interleaver Depth

D. The Effect of Diversity

A common technique to overcome frequency selective fading is the application of diversity. Multipath diversity in WCDMA is commonly achieved in frequency selective fading channels using a RAKE receiver to collect multiple copies of the signal. As shown in [24], the performance of an *L*-branch RAKE receiver in a frequency selective fading channel using MRC is similar to an *L*-th order diversity in which the BER performance is improved by increasing the number of paths. Hence, as expected the 3-path FS fading channel yields a better capacity performance than the FF case. However, in the FS case, unlike the FF case, the orthogonality of spreading codes to each other (including the pilot signal) breaks down hence the cross-correlation values between the intended user's spreading sequence and the sequences of other users and the pilot is no longer zero. This manifests itself as an extra noise which in turn degrades the system performance more. Also, the power delay profile of the FS channel has a large impact on the system performance. Further distortion is added by the optical subsystem which also contributes to the breakdown of orthogonality between sequences.

To verify the above argument, simulations were carried out for the 4-path FS fading channel, i.e. TC/FS(4-path) which exhibits an exponentially decaying power delay profile. The corresponding capacity graphs are shown in Fig. 7 for a 10 ms interleaver depth. Compared to the results for the TC/FS(3-path) channel of Fig. 5, the peak capacity at 0 dB OBO is reduced by 100×(37-29)/37 = 21.6%. This large capacity reduction is attributable to two

effects. Firstly, due to the larger number of paths, the interaction of different spreading codes in the presence of the optical subsystem nonlinearity leads to more distortions in TC/FS(4-path) than TC/FS(3-path). Secondly, the diversity of TC/FS(3-path) with 3 equal power paths is greater than the diversity of TC/FS(4-path). The RAKE receiver offers better performance for the equal-power multipath case. The above argument holds for all OBO.

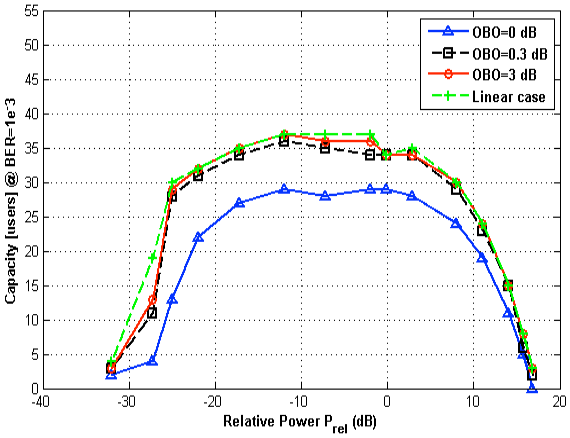

Fig. 7 Capacity vs. P_{rel} for TC/FS(4 Path) Scenario: 10 ms Interleaver Depth

E. The Effect of Estimation Interval

An estimate of the WCDMA channel is obtained by evaluating a portion of the frame over the interval $T_{est} \leq T_{fr}$, which is then applied to whole frame for data recovery. This technique reduces the processing time but the system performance is degraded compared to estimation over a full frame period. In order to investigate the effect of the estimation interval on the system performance, the previous experiments for the TC/FS(4-path) channel (with a TC interleaver depth of 10 ms) were repeated for estimation intervals equal to a slot period (T_{est} = 0.667 ms) and a symbol period (T_{est} = 0.0167 ms). The corresponding capacities are plotted in Fig. 8 for slot level estimation (left pane) and symbol level estimation (right pane). For all OBO levels, the capacity exhibits the same trend as discussed previously. By decreasing the estimation interval, the plots move toward higher pilot power levels. Also, the system capacity is degraded by decreasing the estimation interval. At 0 dB OBO, for example, the peak capacity is decreased from 29 users for frame interval estimation to 27 for slot interval estimation and 26 for symbol interval

estimation. While the peak capacities are slightly reduced with decreasing estimation interval, there is a significant difference in the power required to achieve the peak capacities.

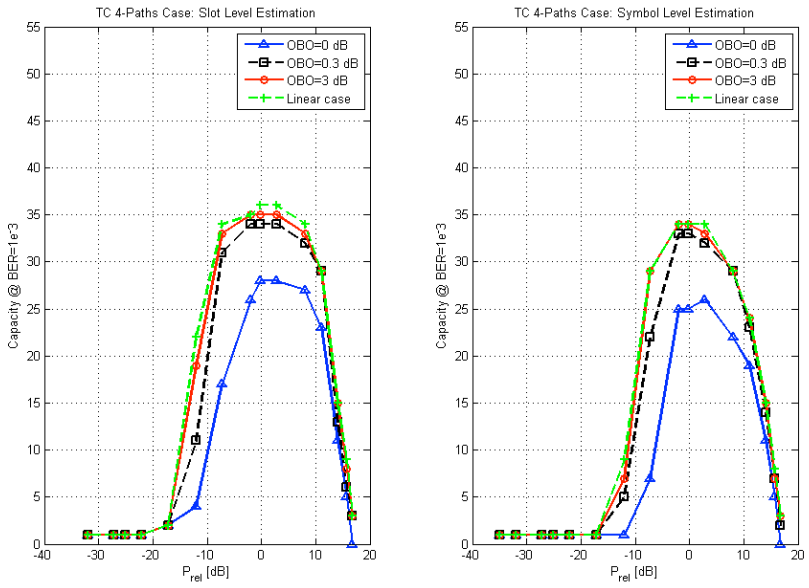

Fig. 8 Capacity vs. P_{rel} for TC/FS(4 Path) Scenario:

Slot Interval Estimation (left pane) and Symbol Interval Estimation (right pane)

In summary, the largest continuous user peak capacity is achieved in the TC/FS(3 path) channel followed by the TC/FS(4 path), TC/FF and CC/FF channels, respectively. Compared to the 3 path FS channel, the 4-path FS channel exhibits a more degraded performance. This is primarily due to the reduction in diversity compared with the 3 path case where all 3 paths have equal power.

Finally, in order to gain insight into the impact of the RoF subsystem and its contribution to performance degradation, the percentage loss of peak capacity due to the optical subsystem compared with a linear system is calculated and summarised in Table IV. Irrespective of the OBO, the TC/FS(3-path) channel incurs the largest loss compared with a linear system followed by the TC/FS(4-path), TC/FF and CC/FF channels, respectively. Nonetheless, while the TC/FS(3-path) channel has the largest capacity loss compared with a linear system, this channel still gives the highest peak capacity of 37 users for 0 dB OBO. Thus, a RoF subsystem has greatest negative

impact on frequency selective channels with the largest diversity. This result suggests that ROF systems inhibit diversity exploitation in wireless communication systems.

The system performance cannot be further improved by the channel estimation technique. Therefore, other techniques such as system equalisation should be used to compensate more fully for all impairments. Nonetheless, it should be emphasised that a 0 dB OBO represents a strong nonlinearity which is not used in practice; instead the optimum quiescent point is determined by a parameter called the Total Degradation [25]. The performance of MIMO based wireless ROF systems is the topic of future research by the authors.

TABLE IV

PEAK CAPACITY LOSS AT BER = 10^{-3}

Case	OBO=0	OBO=0.3	OBO=3
CC/FF	12%	0%	0%
TC/FF	19%	3%	0%
TC/FS(3-Path)	43%	8%	5%
TC/FS(4-Path)	27%	3%	3%

V. CONCLUSION

In this paper, the impact of the optical subsystem nonlinearities on the system capacity performance of a RoF–WCDMA system for different fading channel conditions, coding schemes, interleaver depths, and estimation intervals was investigated. The results demonstrated that pilot aided channel estimation is an effective technique to equalise a signal degraded by optical channel impairments as well as radio channel impairments. The achievable optimum performance depends on the OBO and *R* values. However, there always exists a value of *R* which maximises the capacity performance. Also, there was a negligible decrease in peak capacity when the channel estimation interval was decreased from a frame to a slot to a symbol interval for the same OBO level.

REFERENCES

[1] Al-Raweshidy, H., and Komaki, S.: 'Radio over fiber technologies for mobile communications networks' (Artech House, 2002)

[2] Pinter S. Z., and Fernando, X. N,: 'Estimation and equalization of fiber-wireless uplink for multiuser CDMA 4G networks' IEEE Trans. on Com., 2010, **58**, (6), pp. 1803-1813.

[3] Wake, D., Nkansah, A., and Gomes, N. J.: 'Radio over fiber link design for next generation wireless systems' IEEE J. of Lightwave Technology, 2010, **28**, (16), pp. 2456-2464.

[4] Lim, C., Nirmalathas, A., Bakaul, M., Gamage, P., Lee, K. L., Yang, Y., Novak. D., .and Waterhouse, R.: 'Fiber-Wireless Networks and Subsystem Technologies' J. of Lightwave Technology, 2010, **28**, (4), pp. 390-405.

[5] Develi, I., "Application of multilayer perceptron networks to laser diode nonlinearity determination for radio-over-fibre mobile communications," Microwave and Optical Technology Letters, Vol. 42, No. 5, pp. 425-427 (2004).

[6] Yuksel, M. E., Develi, I., "A neuro-fuzzy computing technique for modeling laser-diode nonlinearity in a radio-over-fibre link," International Journal of RF and Microwave Computer-Aided Engineering, Vol. 15, No. 3, 329-335 (2005).

[7] Niiho, T., Nakaso, M., Masuda, K., Sasai, H., Utsumi, K., and Fuse, M.: 'Transmission performance of multichannel wireless LAN system based on radio-over-fiber techniques' IEEE Trans. on Microwave Theory and Techniques, 2006, **54**, (2), pp. 980 – 989.

[8] Yuen,R., and Fernando, X.: 'Analysis of sub-carrier multiplexed radio over fiber link for the simultaneous support of wlan and wcdma systems' Wireless Personal Communications, Special Issue on Advances on Wireless LANs and PANs, 2005, .**33**, (1), pp. 1–20.

[9] Lin, W.-P., Peng, W.-R., and Chi, S.: 'A robust architecture for wdm radio-over-fiber access networks' Proc. Optical Fiber Communication Conference, Feb. 2004, vol. 2, p. 3.

[10] Fernando, X., Kosek, H., He, Y., and Gu, X.: 'Optical domain demultiplexing of subcarrier multiplexed cellular and wireless lan radio signals' Proc. SPIE Conf., Sep. 2005, pp. 59711S1–59711S10,

[11] Van Nee, R., and Prasad, R.: 'OFDM for Wireless Multimedia Communication' (Artech House, 2000)

[12] Fernando, X. N., and Seasay, A. B.: 'Characteristics of directly modulated RoF Link for wireless access' CCECE2004, 2 5 May 2004, vol. 4, pp. 2167 – 2170.

[13] Baghersalimi, G., O'Farrell, T., and Postoyalko,V.: 'Pilot-aided channel estimation in WCDMA on a radio-over-fibre channel' London Communication Symposium, 2006, pp.25-28.

[14] Zhang, J., He, S., and Yin, S.: 'A memory polynomial predistorter for compensation of nonlinearity with memory effects in WCDMA transmitter' ICCCAS 2009, pp. 913 – 916.

[15] Tachikawa, K.: 'W CDMA mobile communications systems' (John Wiley and Sons, 2002)

[16] Way, W., and Afrashteh, A.: 'Linearity characterization of connectorized laser diodes under microwave intensity modulation by am/am and am/pm measurements' JMTT-S Int. Microwave Symposium Digest, June 1986, vol. 86, issue 1, pp. 659 –662

[17] Bosch, W., and Gatti, G.: 'Measurement and simulation of memory effects in pre- distortion linearizers' IEEE Tran. on Microwave Theory and Techniques, December 1989, **37**, (12), pp. 1885 – 1890.

[18] Lee,, C. H., 'Characterisation and compensation of direct laser modulation nonlinearity in radio-over-fibre systems' PhD thesis, University of Leeds, 2004.

[19] Qaraqe, K. A., and Roe, S.: 'Channel estimation algorithms for third generation W CDMA communication systems' 53rd IEEE Vehicular Technology Conference, 6 9 May 2001, vol. 4, pp. 2675 – 2679.

[20] Rappaport, T. S.: 'Wireless communications: principles and practice' (Prentice Hall, 2002)

[21] 3GPP: ' TS 25.101: UE radio transmission and reception (FDD)', 2006.

[22] 3GPP: 'TS 25.212: Multiplexing and channel coding (FDD)', 2006.

[23] 3GPP: 'TS 25.213: Spreading and modulation (FDD)', 2006.

[24] Tan, C., Ong, L., Yee, M., Luo, B., and Tang, P.: 'Direct transmission of ultra wideband signals using single mode radio over fiber system' Proc. APMC, Dec. 2005, vol 2, p .3.

[25] Fazel, K., and Kaiser, S.: 'Analysis of non-linear distortions on MC-CDMA' IEEE Int. Conf. on Com., June1998, vol. 2, pp. 1028–1034.